Complex coordinates in transformation optics

Bogdan-Ioan Popa* and Steven A. Cummer†
Department of Electrical and Computer Engineering, Duke University, Durham, North Carolina 27708, USA
(Received 19 October 2011; published 16 December 2011)

We show that complex coordinates used in conjunction with transformation optics offer an extra degree of freedom that allows control over not only the propagation direction of electromagnetic waves but also their amplitude. We illustrate this idea in two applications. First, we show that in an n-dimensional space one can manipulate the field amplitude for up to n different amplitude distributions in regions that are critical to the performance of the device under consideration, and thus reduce the device's sensitivity to design imperfections in these regions. Second, we expand previous work on reflectionless perfectly matched layers and show how complex coordinates and transformation optics are a natural choice for designing perfectly matched layers of arbitrary shape.

DOI: 10.1103/PhysRevA.84.063837 PACS number(s): 42.70.−a, 41.20.Jb, 81.05.Xj

I. INTRODUCTION

Transformation optics is a general technique that allows the design of remarkable devices [1,2]. Originally introduced as a means to design scattering reducing coatings, also known as "invisibility cloaks" (see, for example, Refs. [1–12], and also [13–15] for reviews of the field), the method has been shown to be effective for other type of devices such as lenses, beam splitters, concentrators and rotators, illusion optics device, or array antennas [16–24].

Central to the transformation optics method is a choice of coordinate transformations that are essentially used to control the electromagnetic fields inside the design. The vast majority of transformation optics devices reported in the literature are based on real mapping functions. One of the primary things that transformation optics with real mapping functions controls is the phase of the electromagnetic fields. By translating the fields from one location to another, the wave phase is effectively changed by the transformation. However, real coordinate transformations do not offer a simple way of manipulating the field amplitude in a controlled manner.

We show here that the range of transformation optics applications can be extended through the use of complex mapping functions. We show how, in general, the complex coordinates thus obtained are a natural way to control the electromagnetic field amplitude and phase together. In the same way that real coordinate transformations enable one to determine the complicated lossless material parameters for a particular wave device, complex coordinate transformations enable one to design devices that also arbitrarily manipulate wave amplitude in prescribed ways. The resulting material parameters (with loss or gain) are often complicated and would be extremely difficult to derive through another technique. There is, perhaps, one exception: an alternative method that provides similar control over a given distribution of electromagnetic fields, but does not involve coordinate transformations, has been recently proposed [25]. However, a transformation optics type of solution that inherits the advantages of this general design procedure is desirable. We illustrate our approach with two main examples.

First, we show how complex coordinates incorporated into the design of the classical cylindrical invisibility cloak result in an extra degree of freedom that allows us to obtain a device in which the electromagnetic field is exponentially attenuated toward the cloak's inner boundary. The advantage is that fields next to the cloaked object can be made close to zero; therefore, the contribution of the inner region, which is characterized by large, hard to obtain, permittivities and permeabilities, to the overall performance of the design is greatly reduced.

Second, we show how complex coordinates can be used to obtain reflectionless, perfectly matched layers (PMLs) of arbitrary shape, which are very useful in reducing the simulation domain in numerical simulations. Complex coordinates have been employed since the development of the PML concept for Cartesian and, later, cylindrical and spherical coordinates. Teixeira and Chew [26] realized that, in principle, changes in the metric of space through arbitrary curvilinear coordinates could be used to obtain many classes of PMLs. Inspired by the analysis of Texeira and Chew we illustrate how transformation optics and complex coordinates can be employed to design arbitrary shaped PMLs.

II. CONTROLLING THE FIELD AMPLITUDE

Consider the propagation of an electromagnetic wave through an arbitrary, possibly inhomogeneous and anisotropic material. We assume that the material parameters vary smoothly enough so that a propagating wave can be locally approximated as a plane wave in a small neighborhood of every point in the material. This assumption does not reduce the generality of the problem too much since it holds in most practical situations. If we assume $\exp(j\omega t)$ time variation, the wave field components can, therefore, be written in a neighborhood of point $\mathbf{r} \equiv (x,y,z)$ as

$$\mathbf{E}(\mathbf{r}) = \mathbf{E_0}(\mathbf{r})e^{-j\mathbf{k_{loc}}(\mathbf{r})\cdot\mathbf{r}}, \tag{1}$$

where $\mathbf{E_0}$ and $\mathbf{k_{loc}}$ are the local electric amplitude vector and, respectively, wave vector. The magnetic field component is given by a similar expression.

*bap7@ee.duke.edu
†cummer@ee.duke.edu

Transformation optics specifies a systematic way of changing the material parameters of the background medium in order to modify the distribution and shape of a particular electromagnetic wave or field configuration. Suppose we want, instead, to change these material parameters in order to change the amplitude of the wave as it propagates through the medium. In other words, we want to obtain an electric field

$$\mathbf{E}_{\mathbf{desired}}(\mathbf{r}) = M(\mathbf{r})\mathbf{E}(\mathbf{r}), \tag{2}$$

where $M(\mathbf{r})$ is a smooth scalar function that represents the desired amplitude correction factor.

Our purpose is to manipulate the field amplitude through a coordinate transformation $\mathbf{r} \mapsto \boldsymbol{\rho}(\mathbf{r})$ that maps $\mathbf{E}_{\mathbf{desired}}(\mathbf{r})$ to $\mathbf{E}(\boldsymbol{\rho})$. Equation (1), in which we replace $\mathbf{r}$ by $\boldsymbol{\rho}$, suggests that one way to achieve amplitude manipulation is to find a transformation in which $\boldsymbol{\rho}$ has an imaginary component. We, therefore, search for a mapping of the following form

$$\boldsymbol{\rho}(\mathbf{r}) = \mathbf{r} + j\,\boldsymbol{\rho}_{\mathbf{im}}(\mathbf{r}). \tag{3}$$

At this point we are not interested in phase manipulation; therefore, we choose the real component of $\boldsymbol{\rho}$ to be unity mapped. We will see shortly, however, that it is useful to consider general complex mappings in which the real part of $\boldsymbol{\rho}$ is different from $\mathbf{r}$, and express these complex transformations as a combination between transformation (3) and a traditional mapping that performs phase manipulation only.

Under the mapping (3), $\mathbf{E}$ transforms to $\mathbf{E}_{\mathbf{desired}}$ according to

$$\mathbf{E}_{\mathbf{desired}}(\mathbf{r}) = [A^{-1}(\boldsymbol{\rho})]^T\mathbf{E}(\boldsymbol{\rho}), \tag{4}$$

where $A^{-1} = \nabla\boldsymbol{\rho}$ is the Jacobian of $\boldsymbol{\rho}(\mathbf{r})$. It follows from transformation optics that the material parameter tensors that produce the desired field amplitude are given by the well-known equations

$$\{\bar{\bar{\epsilon}}_d, \bar{\bar{\mu}}_d\} = \det(A^{-1})A\{\bar{\bar{\epsilon}}, \bar{\bar{\mu}}\}A^T. \tag{5}$$

Moreover, transformation optics ensures that, as long as $\boldsymbol{\rho}_{\mathbf{im}} = 0$ on the boundary between the region inside which we wish to control the amplitude and the rest of the space, our manipulation of the field amplitude does not result in unwanted scattering off this region.

Next we solve for $\boldsymbol{\rho}_{\mathbf{im}}$ by expanding Eq. (4) with the help of Eqs. (1) and (2). We obtain

$$M(\mathbf{r})\mathbf{E}_{\mathbf{0}}(\mathbf{r}) = [(I_3 + j\nabla\boldsymbol{\rho}_{\mathbf{im}})^{-1}]^T e^{\mathbf{k}_{\mathbf{loc}}(\mathbf{r})\cdot\boldsymbol{\rho}_{\mathbf{im}}(\mathbf{r})}\mathbf{E}_{\mathbf{0}}(\mathbf{r}), \tag{6}$$

where I_3 is the unity matrix. We will see in a number of examples in the remainder of this article that in many situations it is relatively easy to solve the above set of partial differential equations for $\boldsymbol{\rho}_{\mathbf{im}}$.

The above analysis considered directly controlling the amplitude of the electric field (but note that the magnetic field will also change as a result of the coordinate transformation). The magnetic field can be directly manipulated in a similar fashion. In fact, since both the electric E and magnetic H fields transform according to Eq. (4) under a transformation of coordinates, Eqs. (3) through (6) retain the same form and all we need to do is replace the E field with the H field.

III. TWO-DIMENSIONAL FIELDS

We consider next the slightly less general case of transverse electric (TE) two-dimensional fields analyzed extensively in the context of transformation optics. As mentioned in the previous section transverse magnetic (TM) waves will behave identically given the duality of the E and H fields.

For TE waves, the electric field has only one out-of-plane component, i.e., $\mathbf{E} = \hat{\mathbf{z}}E$, and the electromagnetic wave has no out-of-plane variation, i.e., $\partial/\partial z = 0$, so that the design equation (6) reduces to

$$\mathbf{k}_{\mathbf{loc}}(\mathbf{r}) \cdot \boldsymbol{\rho}_{\mathbf{im}}(\mathbf{r}) = \ln[M(\mathbf{r})]. \tag{7}$$

This single linear equation has two unknowns, namely, the components of $\boldsymbol{\rho}_{\mathbf{im}}$, and consequently has multiple solutions. This means that, in general, we can control independently the amplitude behavior of two different waves characterized by different $\mathbf{k}_{\mathbf{loc}}(\mathbf{r})$ distributions traveling through some region of space.

We illustrate the approach described above through the simple example presented in Fig. 1(a) of a cylindrical wave generated by an infinite line source in vacuum. In this case we have $\mathbf{E}_{\mathbf{0}}(\mathbf{r}) = \hat{\mathbf{z}}E_0/\sqrt{r}$ and $\mathbf{k}_{\mathbf{loc}}(\mathbf{r}) = \hat{\mathbf{r}}k_0$ with k_0 the free space wave number.

Suppose we want to modify the amplitude of the electric field inside a circular region of radius R so that the amplitude increases exponentially from the edges of the region toward the center as shown in Fig. 1(b). The correction we want to apply is written as follows:

$$M(\mathbf{r}) = e^{\alpha(R-|\mathbf{r}-\mathbf{r}_0|)}, \tag{8}$$

where $\mathbf{r}_0$ is the position vector of the center of the region, and α controls the rate of amplitude increase. A plot of $M(\mathbf{r})$ is

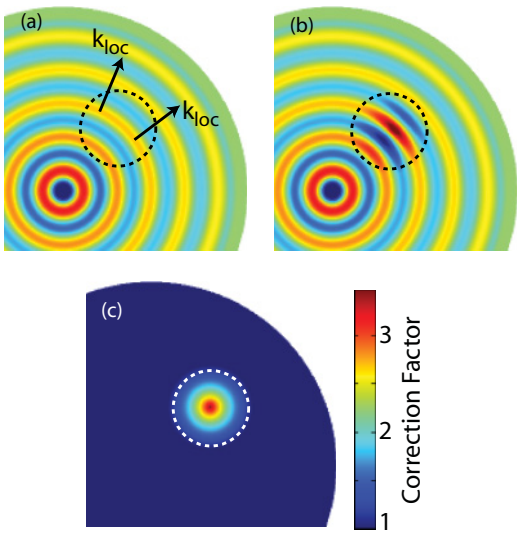

FIG. 1. (Color online) Controlling the electric field amplitude of a TE wave. (a) Electric field component of a cylindrical wave, $\mathbf{E}(\mathbf{r})$; the local wave vectors are highlighted at two points in the domain. (b) Desired electric field behavior, $\mathbf{E}_{\mathbf{desired}}(\mathbf{r})$, i.e., we want the field to be amplified inside the highlighted circular region. (c) Desired amplitude correction factor, $M(\mathbf{r})$.

shown in Fig. 1(c). Equation (7) becomes

$$k_0\hat{\mathbf{r}}\cdot\boldsymbol{\rho}_{\mathbf{im}} = \alpha(R - |\mathbf{r} - \mathbf{r}_0|). \tag{9}$$

One of its possible solutions is

$$\boldsymbol{\rho}_{\mathbf{im}} = \hat{\mathbf{r}}\alpha k_0^{-1}(R - |\mathbf{r} - \mathbf{r}_0|). \tag{10}$$

Having $\boldsymbol{\rho}_{\mathbf{im}}$ determined, we use Eq. (5) to find the material parameters inside the circular region that produce the desired field amplitude. Figure 1(b) shows the electric field distribution computed using Comsol Multiphysics, a commercial solver of Maxwell's equations, which confirms the desired behavior.

We consider next a more interesting example and use it to look at the typical complex valued material parameters that result using this method, and more importantly at their imaginary parts.

IV. CONTROLLING FIELD AMPLITUDE INSIDE AN INVISIBILITY CLOAK

Scattering reducing shells, also known as "invisibility cloaks," have been studied extensively in the context of transformation optics. We show below how amplitude manipulation using complex coordinates can be used to address one of the difficulties related to this type of device.

The two-dimensional cylindrical invisibility cloak, as originally proposed, is designed based on the following mapping:

$$\boldsymbol{\xi} = \mathbf{r}\left(1 - \frac{a}{|\mathbf{r}|}\right)\frac{b}{b-a}. \tag{11}$$

This mapping and the cloak it generates has been extensively analyzed in the literature (see, for example, [1–9]), therefore we will only summarize here its main properties with the help of Figs. 2(a) and 2(b). More specifically, the empty space [Fig. 2(a)] described by the position vector $\boldsymbol{\xi}$ (called virtual space) is mapped into the real space described by the position vector $\mathbf{r}$ [Fig. 2(b)]. The origin of the virtual space is mapped into the circle of radius a centered at the origin of the real space, and represents the boundary of the object to be cloaked. The circle of radius b centered at the origin in the virtual space is mapped into a circle of the same size in the real space, and represents the outer cloak boundary. The cloaked object is a perfect electric conductor (PEC).

Figure 2 shows the electric component of a TE plane wave propagating in the horizontal direction in the virtual space [Fig. 2(a)] being mapped to the corresponding wave in the real space [Fig. 2(b)]. As before, the fields were numerically computed with Comsol Multiphysics. This particular mapping specifies that, at the inner boundary of the cloak, the electric field should have precisely the same value as at the origin of the virtual space, i.e., a nonzero amplitude. On the other hand the cloaked PEC object enforces the field to be exactly zero on the same boundary.

This implies that the material parameters inside the cloaking medium are such that the electric field amplitude decays from its nonzero value everywhere else to zero over a vanishingly small distance on the inner cloak boundary, which in turns means that small deviations from the material parameters at this boundary can result in non-negligible scattering off the cloak. This characteristic, observed by others [5,6,11,14], is seen in Fig. 2(b). The finite mesh used in the simulations is unable to capture this infinitely fast variation, and the result is an artificial, numerically induced, non-negligible scattering. The perfect magnetic conductor on the top and bottom boundaries of the numerical domain make this scattering more visible.

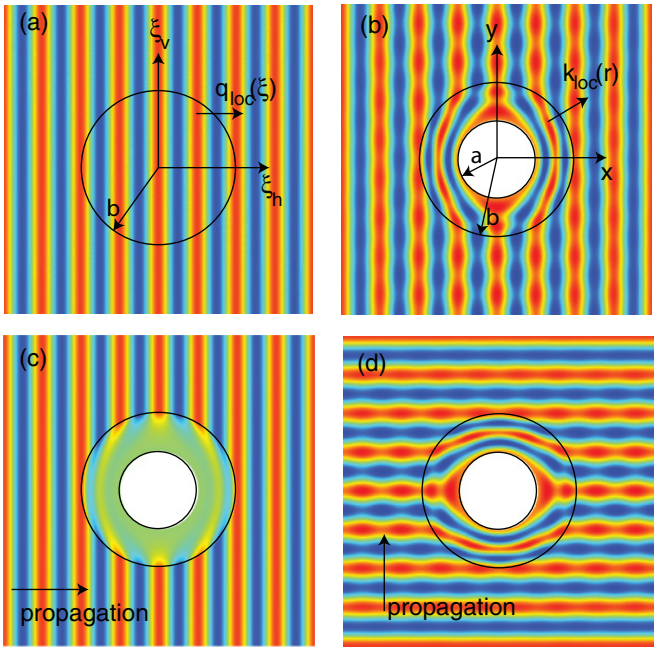

FIG. 2. (Color online) Electric field inside and around the classical and modified cylindrical cloaks. The classical cloak is designed by mapping the free ("virtual") space (a) to the "real" space (b). Large fields in the critical region close to the inner cloak boundary are responsible for the numerical artifacts materialized as visible scattering. An additional mapping based on complex coordinates is used to modify the classical cloak so that a wave propagating horizontally is greatly attenuated at the sensitive inner cloak boundary (c), but the same wave propagating vertically is not affected (d).

We address this issue by employing the complex coordinates method outlined above in order to reduce the fields at the sensitive inner cloak boundary, and with them the unwanted scattering. We can solve, as before, Eq. (7) in order to find the complex transformation that results in the desired field distribution. Even though possible, this direct approach is more involved in this situation because $\mathbf{k}_{\mathbf{loc}}$ inside the cloak has a nontrivial $\mathbf{r}$ variation. Instead it is easier to take advantage of the fact that the fields inside the cloak were mapped from fields of a plane wave traveling in free space as illustrated in Figs. 2(a) and 2(b). This means that we can use a complex mapping $\boldsymbol{\xi} \mapsto \boldsymbol{\rho}(\boldsymbol{\xi}) = \boldsymbol{\xi} + j\boldsymbol{\rho}_{\mathbf{im}}(\boldsymbol{\xi})$ to reduce the fields at the origin of the virtual space, i.e., the region that is mapped to the inner cloak boundary, and combine it with the standard cloak transformation given in Eq. (11). The result is a mapping $\mathbf{r} \mapsto \boldsymbol{\xi}(\mathbf{r}) \mapsto \boldsymbol{\rho}[\boldsymbol{\xi}(\mathbf{r})]$ that produces a device for which the fields toward the inner boundary are significantly attenuated.

Finding the transformation $\boldsymbol{\xi} \mapsto \boldsymbol{\rho}(\boldsymbol{\xi})$ is a problem very similar to that solved in the previous section. More specifically,

we want an amplitude correction

$$M(\boldsymbol{\xi}) = e^{-\alpha(b-|\boldsymbol{\xi}|)}, \tag{12}$$

where α controls the degree of attenuation. Since in free space the local wave vector for a horizontally propagating wave is $\mathbf{q_{loc}} = k_0\hat{\boldsymbol{\xi}}_h$, where $\hat{\boldsymbol{\xi}}_h$ is the unit vector in the horizontal direction, the solution to Eq. (7) is written

$$\boldsymbol{\rho}_{\mathbf{im}} = -\hat{\boldsymbol{\xi}}_h \alpha k_0^{-1}(b - |\boldsymbol{\xi}|) + \hat{\boldsymbol{\xi}}_v f(\boldsymbol{\xi}), \tag{13}$$

where $\hat{\boldsymbol{\xi}}_v$ is the unit vector in the vertical direction and $f(\boldsymbol{\xi})$ is an arbitrary scalar function that can be used to control the amplitude of a wave propagating in another direction. We choose $f(\boldsymbol{\xi}) = 0$ so that the amplitude of a wave propagating in the vertical direction will not be affected by the transformation $\boldsymbol{\xi} \mapsto \boldsymbol{\rho}(\mathbf{r})$.

It is interesting to note that it is not possible to obtain attenuation for all directions of incidence because, once $\boldsymbol{\rho}_{\mathbf{im}}$ is determined, we can always choose an incident wave whose wave vector is perpendicular on $\boldsymbol{\rho}_{\mathbf{im}}$. For that particular wave the complex transformation will have no effect.

The mapping $\mathbf{r} \mapsto \boldsymbol{\rho}$ is obtained from Eqs. (11) and (13) as follows:

$$\boldsymbol{\rho} = \mathbf{r}\left(1 - \frac{a}{|\mathbf{r}|}\right)\frac{b}{b-a} - j\hat{\mathbf{x}}\alpha k_0^{-1}\frac{b}{b-a}(b - |\mathbf{r}|). \tag{14}$$

In the previous equation we took into account that the $\boldsymbol{\xi}$ and $\mathbf{r}$ spaces are Cartesian according to the "materials interpretation" introduced in Ref. [4], and have the same unit vectors $\hat{\mathbf{x}} = \hat{\boldsymbol{\xi}}_h$.

Next we apply Eq. (5) to find the material parameters inside the modified cloak. Figure 3 shows the principal axis components of the permittivity and permeability tensors. We notice the variation of the real part of these parameters typical for a cylindrical cloak.

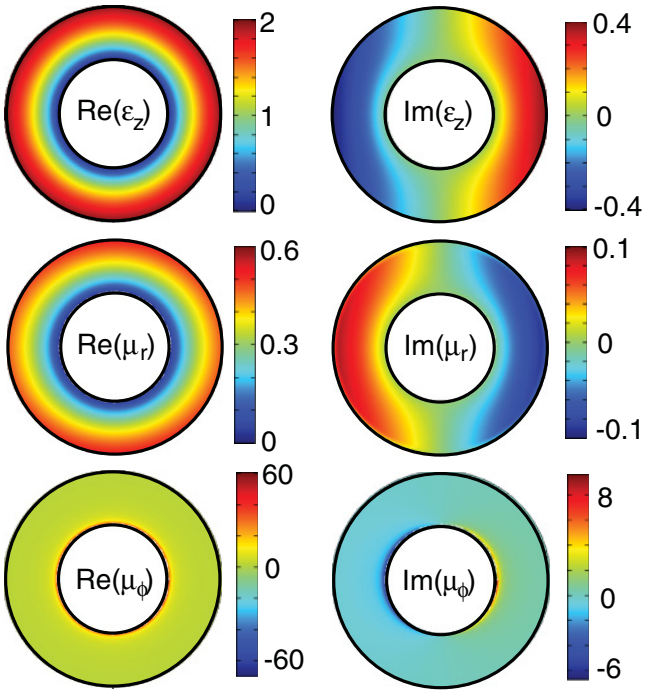

FIG. 3. (Color online) Principal axis relative material parameters, real (left panels) and imaginary (right panels) parts, inside the modified cloak.

The field amplitude inside the shell is controlled precisely through a relatively simple analytic procedure. The end result is a relatively complicated and nonintuitive distribution of the imaginary parts of both the permittivity and permeability that controls the wave amplitude in the desired way and that would be extremely difficult to derive through another approach. Both positive and negative values of the imaginary components of the material parameters are required (i.e., both loss and gain). Despite the important field attenuation, however, these imaginary parts have only a modest variation and are within 10–17% of the corresponding real parts. These material parameters are obtained such that, for horizontal incidence, the wave is attenuated as it propagates along the radial direction and amplified as it propagates along the azimuthal dimension around the cloak.

Figure 2 shows the electric fields obtained inside and around our cloak for an incoming wave propagating in the horizontal [Fig. 2(c)] and vertical [Fig. 2(d)] directions. As expected, in the first case the field amplitude is exponentially attenuated toward the inner boundary of the cloak, and is not affected in the second case. We see in this latter case the small but clearly visible scattering from the device caused by the finite mesh grid at the cloak-object interface where, as explained above, the fields have to decay very rapidly. A comparison between Figs. 2(c) and 2(d) shows that the field attenuation through the complex coordinates technique for horizontal incidence cancels this effect. In both cases the same mesh grid has been used.

As mentioned before, this combination of gain and loss media results in a degree of attenuation in the cloak that depends on the direction of propagation of the incident wave, with one particular direction along which no attenuation takes place. From this point of view, our approach may seem imperfect and is reminiscent of using optimization algorithms [11,27] to trade perfect functionality for device simplicity. Note, however, that unlike the use of optimization algorithms, our approach sacrifices very little functionality: the attenuating cloak is very broadband and works for all incident wave directions of propagation except one.

V. PERFECTLY MATCHED LAYERS OF ARBITRARY SHAPE

As we have seen so far, complex coordinates can be used to reduce the influence of certain device areas susceptible to reduce the effectiveness of the device. Other applications are also possible, for instance, in the area of reflectionless PML design. For example, MEEP [28], a full-wave solver of Maxwell's equations, uses transformation optics techniques to derive the material parameters inside classical PMLs, such as those used in cylindrical and Cartesian coordinate frames. Transformation optics can, however, do more than that.

For complicated shapes, classical PMLs lose effectiveness. Teixeira and Chew [26] showed that complex coordinates in curvilinear coordinate frames could in principle be used to design a large number of classes of PML. Inspired by their analysis, we use complex coordinates and transformation

optics to present a practical way to design a perfectly matched layer that surrounds a domain having an irregular shape.

To keep the method general, we choose PML boundaries whose geometries are too complex to be modeled through analytic equations, as illustrated in Fig. 4(a). Let Ω_i be its interior and Ω_e the exterior boundaries. The only limitation we impose on Ω_e (but not Ω_i) is to enclose a convex volume. The PML is by definition a reflectionless material that absorbs any wave incident on it. Our goal is to find the material parameters inside this material.

To do this we need to find $\boldsymbol{\rho}_{\mathbf{im}}$ satisfying Eq. (6) such that $M(\mathbf{r_e}) < 0$ for all $\mathbf{r_e} \in \Omega_e$ and $\boldsymbol{\rho}_{\mathbf{im}}(\mathbf{r_i}) = 1$ for all $\mathbf{r_e} \in \Omega_i$ and every choice of $\mathbf{E_0}$ and $\mathbf{k_{loc}}$. Since we are not interested in the exact variation of M, but only its subunitary value on the outside boundary of the domain, we can simplify the problem as follows. Thus, we look for a $\boldsymbol{\rho}_{\mathbf{im}}$ whose variation is much slower than that of an exponential, so that the variation of $\nabla \boldsymbol{\rho}_{\mathbf{im}} \exp(\mathbf{k_{loc}} \cdot \boldsymbol{\rho}_{\mathbf{im}})$ is dominated by the exponential. Under this assumption, we can neglect the $\nabla \boldsymbol{\rho}_{\mathbf{im}}$ term in Eq. (6) and the problem reduces to finding $\boldsymbol{\rho}_{\mathbf{im}}$ such that

$$\mathbf{k_{loc}}(\mathbf{r_e}) \cdot \boldsymbol{\rho}_{\mathbf{im}}(\mathbf{r_e}) < 0, \tag{15}$$

for every choice of $\mathbf{k_{loc}}$ corresponding to a wave incident on Ω_e. In the above equation $\mathbf{r_e}$ is an arbitrary point on Ω_e.

Since Ω_e was assumed convex, for every such $\mathbf{k_{loc}}$ we have $\mathbf{k_{loc}} \cdot \hat{\mathbf{n}} > 0$ on Ω_e, where $\hat{\mathbf{n}}$ is the outward pointing unit vector normal to Ω_e; in other words, $\mathbf{k_{loc}}$ and $\hat{\mathbf{n}}$ always form an acute angle at every point of Ω_e. This property allows us to choose the following $\boldsymbol{\rho}_{\mathbf{im}}$ that satisfies Eq. (15):

$$\boldsymbol{\rho}_{\mathbf{im}} = -\alpha \phi \nabla \phi, \tag{16}$$

where α controls the attenuation inside the PML, and $\phi(\mathbf{r})$ is a scalar, positive function for which $\phi(\Omega_i) = 0$ and $\phi(\Omega_e) = 1$. Note that for this solution (which is not unique) $\nabla\phi$ and, consequently, $\boldsymbol{\rho}_{\mathbf{im}}$ are both vectors parallel to $\hat{\mathbf{n}}$. The function ϕ is multiplied by $\nabla\phi$ in order to enforce the constraint $\boldsymbol{\rho}_{\mathbf{im}}(\mathbf{r_i}) = 0$.

Since Ω_i and Ω_e may have geometries too complicated to be modeled through analytic equations, it is more useful to express ϕ as the solution to a differential equation which can be solved numerically. We choose ϕ to be the solution to the Laplace equation $\Delta\phi = 0$, because it is known to provide smooth, slowly varying functions. Interestingly, this particular solution applied to classical Cartesian, cylindrical or spherical PMLs result in the exact same material parameters inside these PMLs that one would obtain with traditional methods.

The function ϕ obtained numerically with Comsol Multiphysics for the example two-dimensional domain of Fig. 4(a) is shown in Fig. 4(b). Having ϕ computed, we can find the Jacobian $\nabla\boldsymbol{\rho}$ corresponding to the mapping given by Eq. (3), and subsequently compute the material parameters inside the PML from Eq. (5).

The constant α determines the amount of wave absorption inside the perfectly matched layer. It is chosen big enough so that the PML attenuates the incoming wave enough to have negligible reflections at the domain outer boundary Ω_e, but small enough to avoid numerical artifacts caused by fields decaying too quickly in regions of space for which the numerical mesh grid is not fine enough. For this particular example we chose $\alpha = 0.05$.

The PML performance of the above example is tested in a numerical simulation by placing a current line source inside the domain bordered by Ω_i. The electric field generated by the source is presented in Fig. 5(a) and shows a clean cylindrical wave propagating away from the source, a testament of excellent PML behavior. In contrast, a typical cylindrical coordinate PML implemented by default in Comsol Multiphysics produces significant reflections back into the domain, which are responsible for the interference pattern visible in Fig. 5(b).

Note that the difference between the effectiveness of the classical PML implemented in Comsol and our design is not mainly related to the degree of attenuation inside the PML, but rather to the direction in which the attenuation is maximum. In a standard cylindrical PML the attenuation is maximum along radial directions starting from a user-defined point. In our simulation we chose this point to be roughly in the center of the domain, and it has coordinates $(0, -4)$. Whenever a wave

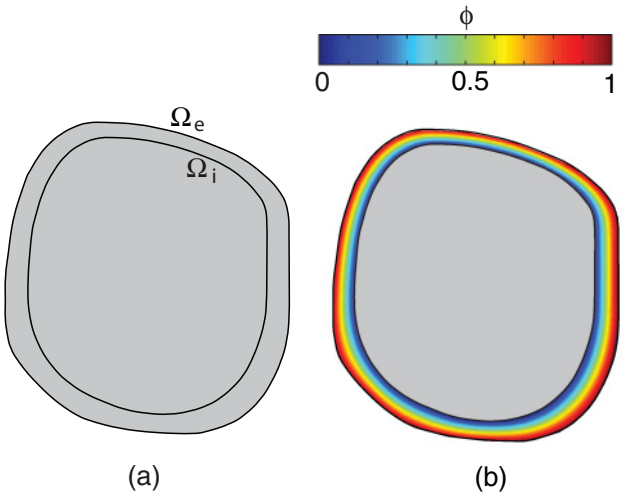

FIG. 4. (Color online) Domain geometry. (a) The PML is situated between the Ω_i and Ω_e curves. (b) Function ϕ inside the PML.

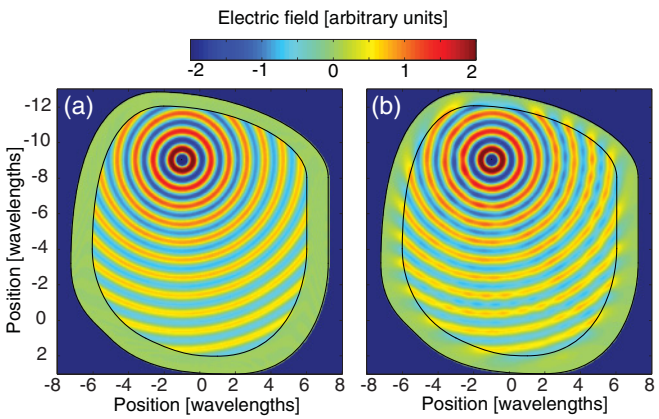

FIG. 5. (Color online) Electric field produced in the numerical domain by a current line source. (a) PML designed using transformation optics. (b) Classical PML implemented in Comsol Multiphysics. Significant scattering off the numerical domain edges is visible in the interference pattern.

inside the domain is such that its local wave vector is almost perpendicular on the radial directions of maximum absorption there will be very little attenuation. This is exactly what we see in Fig. 5(b). In contrast, our PML is designed such that the directions of maximum attenuation, which are given by the $\nabla\phi$ vector, change inside the PML in order to take into account the complex shape of the PML.

An important part of this analysis relies on the numerical domain being convex, in which case Eq. (15) holds for outgoing waves. Concave domains do not satisfy this inequality; therefore, for these domains, some waves hitting the outer PML boundary may be amplified inside the PML, i.e., the electric field on Ω_e may be larger than on Ω_i, or, equivalently, $M(\mathbf{r_e}) > 1$ for some $\mathbf{r_e} \in \Omega_e$. This is consistent with Teixeira and Chew's observation that inner PML layers (which make the domain concave) may not be possible [29].

VI. CONCLUSIONS

We showed that complex coordinates employed in transformation optics provide an extra degree of freedom that allows us to control not only the electromagnetic field spatial distribution but also its amplitude. We illustrated this idea in two typical applications.

The first one featured the manipulation of the field amplitude produced by a particular incident wave. This is desirable when we wish to reduce the sensitivity of some regions of a device to that device's performance. Applying this idea to an invisibility cloak we showed how to reduce the fields inside the cloak in regions of large permittivity and permeability gradients. The second example presented a practical approach to the design of reflectionless, perfectly matched layers for numerical domains of arbitrary shape.

ACKNOWLEDGMENTS

This work was supported by a Multidisciplinary University Research Initiative from the Army Research Office (Contract No. W911NF-09-1-0539) and by a Lockheed-Martin University Research Initiative. The authors thank Charles Chase and Larry Bloxham from Lockheed-Martin for useful discussions.

[1] J. B. Pendry, D. Schurig, and D. R. Smith, Science **312**, 1780 (2006).
[2] U. Leonhardt, Science **312**, 1777 (2006).
[3] D. Schurig, J. J. Mock, B. J. Justice, S. A. Cummer, J. B. Pendry, A. F. Starr, and D. R. Smith, Science **10**, 977 (2006).
[4] D. Schurig, J. B. Pendry, and D. R. Smith, Opt. Express **14**, 9794 (2006).
[5] S. A. Cummer, B.-I. Popa, D. Schurig, D. R. Smith, and J. B. Pendry, Phys. Rev. E **74**, 036621 (2006).
[6] Z. Ruan, M. Yan, C. W. Neff, and M. Qiu, Phys. Rev. Lett. **99**, 113903 (2007).
[7] W. Cai, U. K. Chettiar, A. V. Kildishev, V. M. Shalaev, and G. W. Milton, Appl. Phys. Lett. **91**, 111105 (2007).
[8] Z. Liang, P. Yao, X. Sun, and X. Jiang, Appl. Phys. Lett. **92**, 131118 (2008).
[9] A. Nicolet, F. Zolla, and S. Guenneau, Opt. Lett. **33**, 1584 (2008).
[10] W. X. Jiang, T. J. Cui, G. X. Yu, X. Q. Lin, Q. Cheng, and J. Y. Chin, J. Phys. D **41**, 085504 (2008).
[11] B.-I. Popa and S. A. Cummer, Phys. Rev. A **79**, 023806 (2009).
[12] B.-I. Popa and S. A. Cummer, Phys. Rev. A **82**, 033837 (2010).
[13] H. Chen, C. T. Chan, and P. Sheng, Nat. Mater. **9**, 387 (2010).
[14] Y. Urzhumov, N. B. Kundtz, D. R. Smith, and J. B. Pendry, J. Opt. **13**, 024002 (2011).
[15] A. V. Kildishev and V. M. Shalaev, Phys. Usp. **54**, 53 (2011).
[16] N. Kundtz and D. R. Smith, Nat. Mater. **9**, 129 (2010).
[17] Z. H. Jiang, M. D. Gregory, and D. H. Werner, Phys. Rev. B **84**, 165111 (2011).
[18] M. Rahm, S. A. Cummer, D. Schurig, J. B. Pendry, and D. R. Smith, Phys. Rev. Lett. **100**, 063903 (2008).
[19] M. Rahm, D. Schurig, D. A. Roberts, S. A. Cummer, D. R. Smith, and J. B. Pendry, Photonics Nanonstruct. Fundam. Appl. **6**, 87 (2008).
[20] Y. Luo, H. Chen, J. Zhang, L. Ran, and J. A. Kong, Phys. Rev. B **77**, 125127 (2008).
[21] Y. Lai, J. Ng, H. Y. Chen, D. Z. Han, J. J. Xiao, Z. Q. Zhang, and C. T. Chan, Phys. Rev. Lett. **102**, 253902 (2009).
[22] T. Chen and S.-R. Yu, J. Appl. Phys. **108**, 093106 (2010).
[23] Y. Luo, J. Zhang, L. Ran, H. Chen, and J. A. Kong, IEEE Antenn. Wireless Propag. Lett. **7**, 509 (2008).
[24] B. I. Popa, J. Allen, and S. A. Cummer, Appl. Phys. Lett. **94**, 244102 (2009).
[25] S. A. Tretyakov, I. S. Nefedov, and P. Alitalo, New. J. Phys. **10**, 115028 (2008).
[26] F. L. Teixeira and W. C. Chew, J. Electromagn. Waves Appl. **13**, 665 (1999).
[27] V. M. Garcia-Chocano, L. Sanchis, A. Diaz-Rubio, J. Martinez-Pastor, F. Cervera, R. Llopis-Pontiveros, and J. Sanchez-Dehesa, Appl. Phys. Lett. **99**, 074102 (2011).
[28] MEEP, the open source full-wave solver of Maxwell's equations developed at Massachusetts Institute of Technology [http://ab-initio.mit.edu/meep].
[29] F. L. Teixeira and W. C. Chew, IEEE Trans. Microw. Theor. Tech. **47**, 775 (1999).